Journal of Physics: Conference Series **440** (2013) 012037 doi:10.1088/1742-6596/440/1/012037

The state of nonlinear force-free magnetic field extrapolation

M. S. Wheatland and S. A. Gilchrist

Sydney Institute for Astronomy, School of Physics, The University of Sydney, NSW 2006, Australia

E-mail: m.wheatland@physics.usyd.edu.au

Abstract. Magnetic field extrapolation is the construction of a model solution for the coronal magnetic field in active regions from magnetic boundary data originating close to the Sun's surface. The nonlinear force-free model (in which the electric current density is parallel to the magnetic field) is often adopted to describe the coronal field. The solution of the nonlinear force-free equations is a challenging computational task, and the application of codes to available boundary data has revealed a number of significant problems with nonlinear force-free extrapolation. This paper summarises the present status of coronal field extrapolation, and describes some recent developments.

1. Background

The structure glimpsed in the solar corona during a total eclipse (see Figure 1) is determined by magnetic fields at the Sun's surface. The energy associated with strong fields around sunspots drives large-scale solar activity, namely flares and coronal mass ejections, which produce space weather storms in our local space environment, posing risks to critical communications infrastructure [1].

Solar activity and space weather motivate the modeling of active region magnetic fields. Ideally we would like to use modeling to address fundamental questions concerning the magnetic energy release process underlying solar activity, as well as to improve the accuracy of space weather forecasts.

1.1. Vector magnetogram data

Vector magnetogram data provide a basis for active region magnetic field modeling. The data are derived from determinations of Stokes polarisation profiles for magnetically sensitive lines formed close to the photosphere [2], for fields of view encompassing active regions. Magnetic field values are obtained from the Stokes profiles via "Stokes inversion," a process involving modeling radiative transport of polarised radiation through the magnetised solar atmosphere. It is important to recognise that field values obtained in this way are inferences, not direct measurements or observations, and as such are subject to substantial a priori uncertainty. The field values are highly method- and model-dependent. Additionally, the intrinsic 180° ambiguity in the direction of the component of the field perpendicular to the line of sight must be resolved to obtain unique magnetic field values [3, 4, 5].

Figure 1. The Sun at totality during the eclipse of 14 November 2012, photographed from Palm Cove beach by the author.

The resulting vector magnetogram data consist of a photospheric map of magnetic field values $\mathbf{B} = (B_x, B_y, B_z)$ over a region at the photosphere, where x, y, and z are local heliocentric coordinates, with z denoting the local radial direction. It is common to neglect the curvature of the photosphere for data on an active region scale, and to refer to z as the vertical direction.

Two space-based vector magnetographs – the Solar Optical Telescope/Spectro-Polarimeter (SOT/SP) on the Hinode satellite [7], and the Helioseismic & Magnetic Imager on the Solar Dynamics Observatory (SDO/HMI) – are now providing data with unprecedented quality, resolution, and cadence [8].

In principle, the data provide boundary conditions for coronal field modeling. Assuming the field is static, a specific coronal field model may be solved as a boundary value problem, a process often called "coronal field reconstruction." The vertical current density J_z at the photosphere provides an important boundary value for coronal field models, which determines the magnetic energy of a solution to the model (the minimum energy magnetostatic field with a prescribed normal component of the field in the boundary is the potential or current-free field, for which $J_z = 0$ in the boundary [6]). The vertical electric current density at the photosphere may be estimated from vector magnetogram data using

$$\mu_0 J_z|_{z=0} = \left[\frac{\partial B_y}{\partial x} - \frac{\partial B_x}{\partial y}\right]_{z=0}. \tag{1}$$

1.2. The nonlinear force-free model

The coronal magnetic field is often modeled as a nonlinear force-free field [9], described by

$$\mathbf{J} \times \mathbf{B} = 0 \quad \text{and} \quad \nabla \cdot \mathbf{B} = 0. \tag{2}$$

The model describes a static coronal field in which the electric current density $\mathbf{J} = \mu_0^{-1} \nabla \times \mathbf{B}$ is everywhere parallel to $\mathbf{B}$. Equations (2) may be rewritten in the form

$$\mathbf{B} \cdot \nabla \alpha = 0 \quad \text{and} \quad \nabla \times \mathbf{B} = \alpha \mathbf{B} \tag{3}$$

by introducing the force-free parameter α, defined by $\mathbf{J} = \alpha \mathbf{B}/\mu_0$. Physically α represents the constant ratio of the electric current density to the magnetic field along a field line. Equations (3) are a coupled system of four nonlinear PDEs for the four dependent variables (B_x, B_y, B_z, and α), which may be solved subject to suitable boundary conditions.

The boundary value problem in a half space ($z > 0$) requires specification of the normal component of the field B_z over the boundary $z = 0$, together with the specification of α over one polarity of the field in the boundary (i.e. the values of α must be given over $z = 0$ where $B_z > 0$, or the values of α must be given over $z = 0$ where $B_z < 0$) [10]. It is necessary only to specify α over one polarity because α is a constant along field lines ($\mathbf{B} \cdot \nabla \alpha = 0$), so values at one polarity are "mapped" to the other polarity by the field lines of the solution. We refer to the polarities defined by $B_z > 0$ and $B_z < 0$ as P and N respectively.

A variety of methods of solution of Equations (3) have been developed [9]. All methods are iterative, and work by solving a system of linear equations, such that an iterative sequence of solutions converges to a solution to the nonlinear Equations (3). Popular methods include Grad-Rubin iteration [10, 11], optimization [12, 13], and the magnetofrictional method [14, 15].

Some force-free methods (e.g. optimization) use the vector field values $\mathbf{B} = (B_x, B_y, B_z)$ at $z = 0$ over both polarities (P and N) as boundary conditions. This is formally an over-prescription, but should lead to no error provided the boundary conditions are consistent with a solution to the force-free model.

The Grad-Rubin scheme requires solution, at at iteration k, of the linear system

$$\mathbf{B}^{[k-1]} \cdot \nabla \alpha^{[k]} = 0 \quad \text{and} \quad \nabla \times \mathbf{B}^{[k]} = \alpha^{[k]} \mathbf{B}^{[k-1]}. \tag{4}$$

The boundary conditions are imposed on $B_z^{[k]}$ at $z = 0$, and on $\alpha^{[k]}$ at $z = 0$ over either P or N, as explained above. The iteration sequence is typically started with a potential (current-free) field for $\mathbf{B}^{[0]}$. A fixed point of the iteration scheme defined by Equations (4) is clearly a solution to the nonlinear force-free equations.

2. The inconsistency problem

2.1. The problem

A sequence of yearly workshops was organised by Lockheed Martin for the years 2005 to 2009, directed at improving the state of nonlinear force-free modeling. The workshops revealed that force-free methods work for test cases but fail, in specific ways, when applied to vector magnetogram data [16, 18, 17, 19]. A basic problem is that the boundary data are inconsistent with the model. Vector magnetogram data provide two sets of boundary conditions for the force-free model, since values of $\alpha = \mu_0 J_z/B_z$ may be determined for both the P and N polarities over the magnetogram field of view. This admits the possibility of two different solutions (the P and N solutions) to the model, depending on the choice of polarity for the boundary conditions. The workshops showed that two distinctly different solutions were obtained, for the Hinode SOT/SP vector magnetograms used in the studies. The field line configurations for the P and N solutions were found to be significantly different, and moreover the magnetic energies of the two solutions were substantially different [17, 19]. Vector magnetogram data typically fail to meet necessary conditions for the existence of a force-free solution [20], which may be attributed to non-magnetic forces at the photospheric level of the atmosphere. The solar atmosphere is thought to become force-free $\approx 400\,\mathrm{km}$ above the photosphere [21].

Figure 2 illustrates the inconsistency problem. The left hand diagram shows field lines for a P solution, and the right hand diagram shows field lines for an N solution, for boundary data which are inconsistent with the force-free model. The field line configurations are distinctly different:

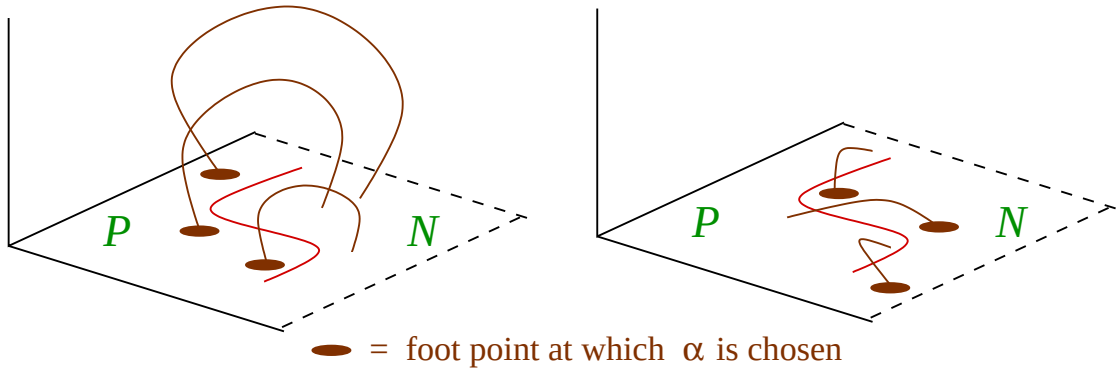

Figure 2. A schematic illustration of the inconsistency problem in nonlinear force-free modeling. If the boundary data are inconsistent with the force-free model, the P and N solutions (left and right diagrams, respectively) will be different. The field lines for the two solutions are shown by the loops.

the P solution has tall, nearly current-free loops over the neutral line separating the polarities, and the N solution has low current-carrying loops which are strongly sheared along the neutral line. This situation may occur if the α values are systematically larger in the N polarity than the P polarity. (Note that an extreme case of inconsistency is shown, for illustration. Actual solar data are unlikely to show systematic discrepancies.)

We would like to estimate the free magnetic energy of the extrapolated solutions, i.e. the energy $E_f = E - E_0$, where E is the total magnetic energy, and E_0 is the energy of the potential field configuration with the same boundary conditions on B_z. However, in general the P and N solutions obtained from extrapolating vector magnetogram data have different magnetic energies. Typically $E_f \ll E_0$, so the free magnetic energy of the P and N solutions may differ by a large factor, as illustrated by an example presented in Section 3.

This discussion applies to methods of solution of the model using values of α over one polarity as boundary conditions. Some methods of solution of the nonlinear force-free model use values of $\mathbf{B}$ over both P and N as BCs. In that case the inconsistency of the boundary data with the model leads to "solutions" with $\mathbf{J} \times \mathbf{B} \neq 0$ and/or $\nabla \cdot \mathbf{B} \neq 0$ somewhere in the coronal volume.

2.2. Practical methods of resolution

The "preprocessing" procedure [22] provides one method of improving (but not resolving) the inconsistency problem. The vector field components in the boundary are modified to meet certain conditions necessary for the force-free model. However, the conditions imposed are not sufficient to ensure a solution to the model, and in general preprocessed boundary data remain inconsistent with the model. The procedure is found to improve results in some cases [19].

A solution consistent with the model is obtained by the "self-consistency procedure" [23, 24], which works as follows. The vector magnetogram data are used to calculate P and N solutions. The two solutions are then used to identify a single force-free solution which is in some sense "closest" to the P and N solutions, and in particular has a very similar mapping of foot points between polarities. The method treats the P and N solutions as equally valid, except that uncertainties in boundary values of α are taken into account (preference is given to boundary data with small uncertainties). The self-consistent solution has the same boundary conditions on B_z as the vector magnetogram, but modified BCs on α.

To give a more detailed account, there are three steps in the self-consistency procedure. Step 1. is the calculation of the P and N solutions, from (unpreprocessed) vector magnetogram data.

The Grad-Rubin scheme of Equation (4) is used [11]. Step 2. is an adjustment of the boundary values, taking uncertainties in α values into account, as follows. Each solution defines a mapping of α values from one polarity to the other, since α is a constant along field lines in a force-free solution (the P solution maps boundary values of α from the P to the N polarity, and the N solution maps boundary values of α from N to P). The mappings define two complete sets of boundary values of α, which we denote by α_P and α_N. (The α_P data consist of the magnetogram values over the P polarity, and mapped values over the N polarity, and the α_N data consist of the magnetogram values over the N polarity, and mapped values over the P polarity.) There are also two complete sets of corresponding uncertainties, σ_P and σ_N, since the uncertainties map also along field lines. Together there are two possible sets of boundary values and uncertainties:

$$\alpha_P \pm \sigma_P \quad \text{and} \quad \alpha_N \pm \sigma_N \quad \text{at } z = 0. \tag{5}$$

The two sets of values are regarded as two (imperfect) determinations of the true values. A Bayesian estimate of the true values and associated uncertainties, assuming Gaussian-distributed errors, is [23]:

$$\alpha_{\rm est} = \frac{\alpha_P/\sigma_P^2 + \alpha_N/\sigma_N^2}{1/\sigma_P^2 + 1/\sigma_N^2} \quad \text{and} \quad \sigma_{\rm est} = \frac{1}{\sqrt{1/\sigma_P^2 + 1/\sigma_N^2}}. \tag{6}$$

The values $\alpha_{\rm est}$ will in general still be inconsistent with the force-free model, but they are expected to be closer to consistency. Step 3. is the process of iteration. Steps 1. and 2. are repeated, with the vector magnetogram-derived values of α replaced by the new estimates $\alpha_{\rm est} \pm \sigma_{\rm est}$. (The first step in the next iteration is the calculation of P and N solutions using the magnetogram boundary values of B_z together with the new boundary values $\alpha_{\rm est}$ for the force-free parameter.)

In practice the self-consistency procedure is found to arrive at a self-consistent solution within about a dozen "cycles" of the three steps (the iterations of the steps are termed cycles to distinguish them from the iterations of the Grad-Rubin procedure used to construct the P and N solutions). A practical convergence criterion for the slef-consistency cycles is that the P and N solution energies agree to $\lesssim 1\%$ for consecutive cycles.

Other approaches to the inconsistency problem have also been presented, in particular an "optimization Grad-Rubin method" [25], and an optimization method incorporating measurement errors [26].

3. A modeling example

To illustrate the application of the self-consistent modeling procedure, we consider the treatment of active region 11029, a small but highly-flare productive region which emerged on the disk on 21-22 Oct 2009. The region produced 73 GOES events above B class during its transit of the disk, briefly interrupting the extended minimum at the end of cycle 23. Because it flared in relative isolation, active region 11029 provided a good subject for a study of the statistics of flare occurrence in an individual active region [27]. The size distribution of soft X-ray events in the region appeared to show a relative deficit of large events – a departure from the well known power-law flare frequency-size distribution. In a follow-up study the region was modeled using the self-consistency procedure, to attempt to determine the region's free energy [28].

Figure 3 shows the data and the results of the nonlinear force-free modeling of the region. The upper left panel illustrates the boundary conditions, which use Hinode SOT/SP vector field determinations together with Solar and Heliospheric Observer/Michelson Doppler Interferometer (SoHO/MDI) line-of-sight magnetic field data [29]. The upper sub-panel shows B_z and the lower sub-panel shows J_z. Uncertainties are assigned to the data based on uncertainties from the Stokes inversion procedure. The upper right panel in Figure 3 demonstrates the convergence of the self-consistency procedure. The energy of the P and N solutions calculated at each self-consistency

cycle is plotted versus the cycle number (the P energies are shown by plus signs and a dashed line, and the N energies are shown by diamonds and a solid line) with the energy given in units of the potential-field energy E_0. Initially the P and N solutions have very different energies, illustrating the inconsistency, but after 10 cycles the energies are very similar, as expected for a self-consistent solution (i.e. one for which the P and N solutions match). The lower panel shows the magnetic field configurations after 10 self-consistency cycles. The view looks down on the computational domain. The boundary values of B_z are shown by the color image, with regions in the P polarity colored blue, and regions in the N polarity colored red. The corresponding field lines for the P and N solutions are shown by the blue and red curves respectively. There is a good correspondence between the two solutions, demonstrating the achievement of a self-consistent solution. (Some discrepancy is seen for longer field lines.)

The calculation was performed on a $440 \times 300 \times 200$ grid with 20 Grad-Rubin iterations per self-consistency cycle. The code is a parallel implementation for shared memory multi-processor computers.

The modeling of active region 11029 allows estimation of the magnetic free energy from the extrapolated solutions. The energy of the self-consistent solution illustrated in Figure 3 is $E/E_0 = 1.04$ (see the top right panel of Figure 3), i.e. the free magnetic energy is $\approx 4\%$ higher than the potential energy. In absolute terms the potential field energy is $E_0 = 1.7 \times 10^{33}$ erg (a relatively large value) and the free energy is $E_f = E - E_0 = 6 \times 10^{31}$ erg. Varying the details of the modeling leads to slightly different self-consistent solutions, with slightly different energies. Based on a sequence of self-consistent calculations the free energy is estimated to lie in the range $E_f = 6 \times 10^{31} - 8 \times 10^{31}$ erg [28]. This example shows that reliable estimation of the magnetic free energy is difficult. Other recent detailed modeling studies confirm this [30].

A self-consistent solution is obtained for active region 11029, but it is unclear whether the model solution provides a close match to the actual coronal magnetic field at the time of the observations. The criteria for validating the modeling in this study are consistency and robustness of the solutions. However, comparison with independent data is needed to confirm the accuracy of the modeling. It is difficult to validate magnetic field extrapolation. Extrapolated field lines may be compared, in projection, with coronal loops in short wavelength images of the corona, but this test is qualitative. In some cases, the three-dimensional trajectories of model field lines have been compared with stereoscopically determined coronal magnetic loop trajectories [19]. It is fair to say that the validation of magnetic field extrapolation remains an outstanding problem.

4. Recent developments

4.1. Extrapolation in spherical geometry

The Helioseismic and Magnetic Imager on the Solar Dynamics Observatory is providing full disk vector magnetogram data [8]. In principle this allows extrapolation of coronal magnetic fields from full disk data, for a given magnetic field model in spherical geometry.

Spherical force-free codes have been developed, for example a generalisation of the optimization method [31, 32], and a new force-free electrodynamics method [33].

Here we provide a brief report on a new implementation of a Grad-Rubin solution to the force-free equations in spherical geometry, which is similar in approach to the existing cartesian code [11]. The method achieves an iterative solution of Equations (3) in spherical polar coordinates, representing the field using a vector potential to ensure $\nabla \cdot \mathbf{B} = 0$. The current updating step [the first of the first of Equations (3)] is achieved via field line tracing, and the field updating step [the second of Equations (3)] uses a Fourier solution of the vector Poisson equation for the vector potential. The boundary conditions are the specification of B_r at the solar surface $r = R_\odot$, the specification of α over one polarity of the radial field at $r = R_\odot$, and the requirement that $\mathbf{B} \to 0$ as $r \to \infty$.

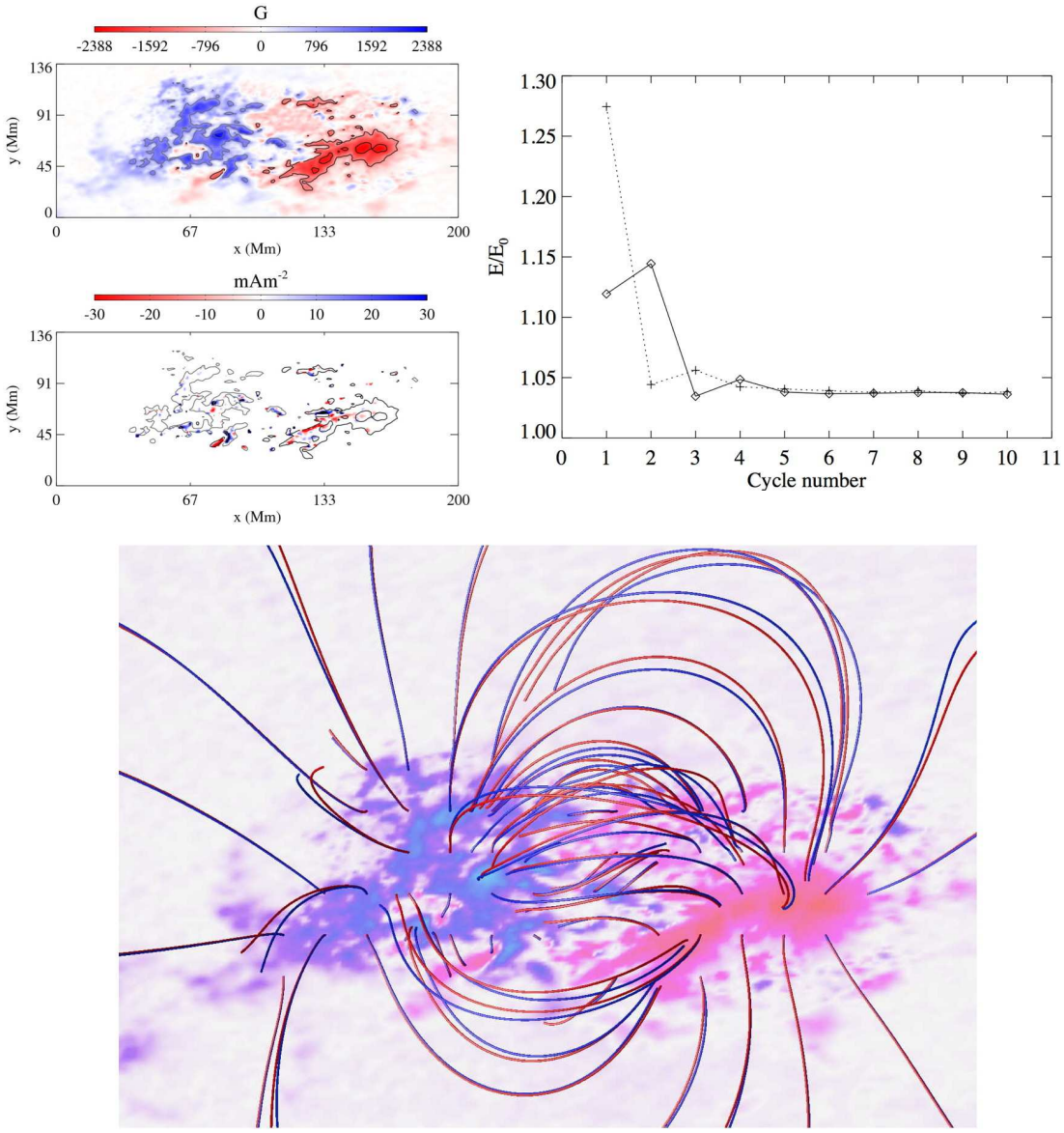

Figure 3. Self-consistent nonlinear force-free modeling of active region 11029 [28]. The upper left panel (with two sub-panels) shows the boundary data, the upper right panel illustrates the achievement of a self-consistent solution, and the lower panel shows the final magnetic field configuration. (See Section 3 for details.)

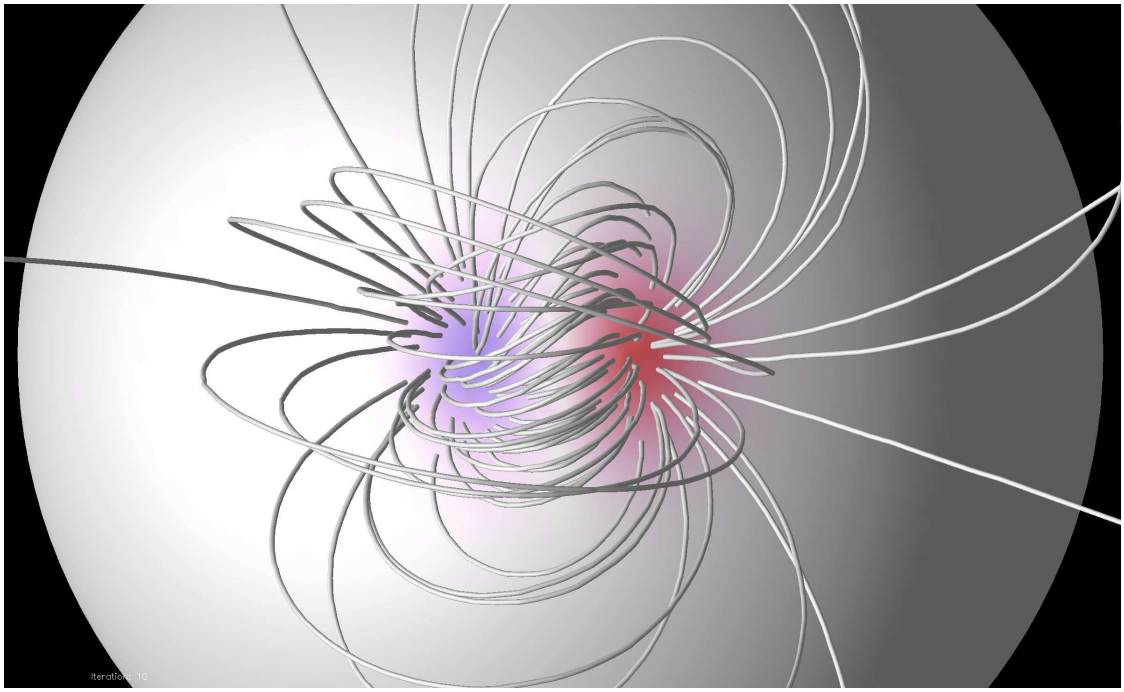

Figure 4. A test of a new full-Sun nonlinear force-free magnetic field calculation code, for a localised current-carrying bipole field configuration (see text).

Figure 4 shows a test calculation using the new code, for a localised current-carrying bipole field configuration. The radial field at the Sun's surface is shown by the color on the sphere (blue for a positive polarity radial field, and red for negative polarity). The boundary field consists of two Gaussian spots at the points $(R_\odot, \phi_1, \theta_1)$ and $(R_\odot, \phi_2, \theta_2)$, where ϕ and θ denote the usual azimuthal and polar angles in spherical polar coordinates. More precisely the radial magnetic field over the model photosphere is

$$B_r(\theta, \phi) = B_0 \left(e^{-s_1^2/\sigma^2} - e^{-s_2^2/\sigma^2} \right), \tag{7}$$

where B_0 is a normalisation constant, and where σ sets the widths of the spots. The variables $s_1 = s_1(\theta, \phi)$ and $s_2 = s_2(\theta, \phi)$ are arc lengths along great circles, given by

$$s_1 = R_\odot \cos^{-1}[\sin\phi_1 \sin\phi + \cos\phi \cos\phi_1 \cos(\theta - \theta_1)], \tag{8}$$

and

$$s_2 = R_\odot \cos^{-1}[\sin\phi_2 \sin\phi + \cos\phi \cos\phi_2 \cos(\theta - \theta_2)]. \tag{9}$$

The boundary condition on electric current is $\alpha = \alpha_0$ where $B_r > 0.9B_0$, and $\alpha = 0$ otherwise, which introduces current at the centre of the positive polarity bipolar spot. (The P solution is calculated in this test case.) The white curves in Figure 4 show the field lines of the field obtained after convergence of a sequence of Grad-Rubin iterations. A force-free twisted bipolar structure is obtained.

4.2. New nonlinear force-free modeling workshops

As mentioned in Section 2, a series of nonlinear force-free modeling workshops was held 2005-2009, organised by Lockheed-Martin personnel, to test and compare extrapolation

methods. The workshops have been relatively influential: the four publications from the workshops [16, 18, 17, 19] have more than 400 citations, and techniques from the papers, e.g. the use of metrics to compare vector field calculations, have become standard.

A new series of workshops will start in 2013, funded by an International Space Sciences Institute (ISSI) International Teams in Space and Earth Sciences grant awarded in 2012 to Marc De Rosa and Mike Wheatland ("Nonlinear Force-Free Modeling of the Solar Corona: Towards a New Generation of Methods"). The workshops will permit testing of recent developments in extrapolation, using Hinode and SDO/HMI data, and the results will be published in Space Science Reviews. The first meeting is scheduled for late 2013.

5. Summary and conclusions

This paper presents an overview of the state of coronal magnetic field extrapolation. The modeling is motivated by a need to understand solar activity, and the potential for improved space weather prediction.

The data used are from vector magnetograms, which are determinations of all three components of the photospheric magnetic field over areas on the Sun including active regions. The model described here is the nonlinear force-free model.

The nonlinear force-free model is popular, but the application of the model to the data presents a variety of challenges. In particular the solar data are inconsistent with the model, leading to unreliable results, as highlighted in a series of nonlinear force-free workshops held during 2005-2009.

Approaches to the inconsistency problem are here discussed, with a focus on the "self-consistency procedure." The method is illustrated in application to active region 11029, a small but flare-productive region observed in late 2009. The modeling of active region 11029 emphasizes the difficulties of estimating the free magnetic energy based on extrapolated solutions, and of validating the solutions.

Two recent developments are also discussed: a new spherical extrapolation method, suitable for application to full-disk vector magnetic field data, and a new series of International Space Science Institute (ISSI) workshops on nonlinear force-free modeling due to start in 2013.

There has been progress in recent years in coronal magnetic field extrapolation, but the state of the art remains unsatisfactory. There are problems associated with the reliability of the data, the ability of the codes to solve the model, the inconsistency of the available data with the model, and we lack ways to confirm results. At this stage extrapolation techniques are not standard packages ready to be included in data processing pipelines: caveat emptor! It is hoped that additional work and new developments will produce reliable methods of extrapolation, for general application.

Acknowledgments

Mike Wheatland thanks the organisers of the meeting. S.A. Gilchrist acknowledges the support of an Australian Postgraduate Research Award. We thank an anonymous referee for a careful reading of the paper.

References

[1] Committee On The Societal and Economic Impacts Of Severe Space Weather Events 2008 *Severe Space Weather Events: Understanding Societal and Economic Impacts Workshop Report, Space Studies Board ad hoc Committee: A Workshop* (Washington: The National Academies Press) DC ISBN: 978-0-309-12769-1
[2] Del Toro Iniesta J C 2003, *Introduction to Spectropolarimetry* (Cambridge: Cambridge University Press) UK ISBN: 0521818273
[3] Metcalf T R 1994 *Sol. Phys.* 155 235
[4] Metcalf T R et al. 2006 *Sol. Phys.* **237** 267
[5] Leka K D Barnes G Crouch A D Metcalf T R Gary G A Jing J Liu Y 2009 *Sol. Phys.* **260** 83

[6] Sakurai T 1979, *Proc. Astronom. Soc. Jap.* **31** 209
[7] Tsuneta S et al. 2008 *Sol. Phys.* **249** 167
[8] Schou J et al. 2012 *Sol. Phys.* **275** 229
[9] Wiegelmann T and Sakurai, T 2012 *Living Rev. Sol. Phys.* 9 5
[10] Grad H and Rubin H 1958 *Proc. 2nd Int. Conf. on Peaceful Uses of Atomic Energy* vol 31 (Geneva: UN) 190
[11] Wheatland M S 2007 *Sol. Phys.* **245** 251
[12] Wheatland M S Sturrock P A Roumeliotis G 2000 *Astrophys. J.* **540** 1150
[13] Wiegelmann T 2008 *J. Geophys. Res. (Space Phys.)* **113** 3
[14] Chodura R and Schlueter A 1981 *J. Computational Phys.* **41** 68
[15] Valori G Kliem B Keppens R 2005 *Astron. Astrophys.* **433** 335
[16] Schrijver C J De Rosa M L Metcalf T R Liu Y McTiernan J Régnier S Wheatland M S Wiegelmann T *Sol. Phys.* **235** 161
[17] Schrijver C J et al. 2008 *Astrophys. J.* **675** 1637
[18] Metcalf T R et al. 2008 *Sol. Phys.* **247** 269
[19] De Rosa M L et al. 2009 *Astrophys. J.* **696** 1780
[20] Molodenskii M M 1969 *Sov. Astron.* **12** 585
[21] Metcalf T R Jiao L McClymont A N Canfield R C Uitenbroek H 1995 *Astrophys. J.* **439** 474
[22] Wiegelmann T Inhester B Sakurai T 2006 *Sol. Phys.* **233** 215
[23] Wheatland M S Régnier S 2009 *Astrophys. J.* **700** L88
[24] Wheatland M S Leka K D 2011 *Astrophys. J.* **728** 112
[25] Amari T Aly J J 2010, *Astron. Astrophys.* **522** A52
[26] Wiegelmann T Inhester B 2010 *Astron. Astrophys.* **516** A107
[27] Wheatland M S 2010 *Astrophys. J.* **710** 1324
[28] Gilchrist S A Wheatland M S Leka, K D 2012 *Sol. Phys.* **276** 133
[29] Scherrer P H et al. 1995 *Sol. Phys.* **162** 129
[30] Wiegelmann T Thalmann J K Inhester B et al. 2012 *Sol. Phys.* **281** 37
[31] Wiegelmann T Neukirch T Ruan P Inhester B 2007 *Astron. Astrophys.* **475** 701
[32] Tadesse T Wiegelmann T Inhester B 2009 *Astron. Astrophys.* **508** 421
[33] Contopoulos I 2012 *Sol. Phys.* **250** DOI 10.1007/s11207-012-0154-y